encit 2020

ABCM Associação Brasileira de Engenharia e Ciências Mecânicas

18th Brazilian Congress of Thermal Sciences and Engineering
November 16-20, 2020 (Online)

ENC-2020-0183
THEORETICAL ANALYSIS OF LIQUID FILM SENSORS BASED ON ELECTRICAL CONDUCTANCE

Victor E. C. Baptistella
Gherhardt Ribatski
Heat Transfer Research Group, São Carlos School of Engineering, University of São Paulo, São Carlos, SP, Brazil
victor.baptistella@usp.br
ribatski@sc.usp.br

Abstract. *The liquid film plays an important role in the characterization of two-phase annular flows. The mean thickness, the presence of waves, their height, frequency, and velocity influence heat transfer rate, critical heat flux and pressure drop. Although it has been widely studied for conventional-sized channels, there is a lack of studies concerning liquid film characterization in mini and microchannels, due to the inherent difficulties associated to small scale conditions. In the present paper, a theoretical analysis is performed of different configurations of micro sensors applied to the measurement of the liquid film thickness based on its electric conductance. This analysis is performed based on results for the average film thickness in microchannels estimated based on different modelling approaches from literature.*

Keywords: *microchannel, liquid film thickness, annular flows, dryout, flow boiling.*

1. INTRODUCTION

The demand to dissipate high heat fluxes in devices of reduced dimensions, such as embedded electronics and high concentration solar systems led to the development of new cooling techniques other than forced convection of air. Phase-change heat transfer in microchannels became a viable solution because it provides high heat transfer coefficients (HTC), low temperature gradients along the heated surface, low refrigerant inventory and high heat transfer area to volume ratios (Ribatski et al. (2007)). In channels of reduced dimensions, according to Tibiriça and Ribatski (2014), the annular flow pattern prevails, with the transition from churn to annular flow probable to occur for vapor qualities lower than 0.2. This flow pattern is characterized by a thin liquid film adjacent to the wall and a vapor core at the center of the duct, which provides high HTCs, but the pressure drop is also high and there is the possibility of wall dryout, with the heat transfer mechanism changing from the highly efficient thermal conduction through the liquid film and evaporation at the vapor-liquid interface to forced convection to the vapor phase, which provides much lower HTCs. Due to the relevance of the liquid film on heat transfer and pressure drop in annular flows, different techniques have been developed to investigate its characteristics. A broad review on δ measurement methods applied to microscale, encompassing acoustic, electric, optic and radiation attenuation methods, is given in Tibiriça et al. (2010). It is pointed out that acoustic and radiative techniques are not suitable for thin, non-planar films, because they possess low temporal resolution and low signal-to-noise ratios, while electrical and optical methods provide spatial and time resolution suitable for thin film measurements. Therefore, the techniques most frequently used are based on the relation of the electrical conductance of the liquid film with its thickness, the reflection of light rays at the gas-liquid interface or the fluorescence of seed particles added to the liquid, viewed by a camera.

Different configurations of conductance sensors have been utilized to investigate two-phase flows, such as parallel wire probes (Han et al. (2006) and Wang et al. (2019)), flush-wire probes (Kang and Kim (1992)) and flush-mounted conductance sensors (Sawant et al. (2008), Damsohn and Prasser (2009) and D'Aleo et al. (2013)). Except flush-mounted sensors, the configurations are intrusive to the flow and are not recommended for microscale flows instrumentation. Still, they are widely used and provide valuable information regarding δ, wave velocity, periodicity, and structure in two-phase flows in macrochannels.

Damsohn and Prasser (2009) and Zhao et al. (2013) evaluated δ using flush-mounted conductance sensors in adiabatic air-water flows in conventional-sized channels. The latter used interdigitated electrodes made of circular disks, circled by ring electrodes (ring-island - RI), while the former used non-interdigitated circular electrodes (island-island - II). By using multiple sensors at different locations from the inlet, it was concluded that: (i) the disturbance wave frequency increases with both air and water superficial velocities, (ii) the frequency of the waves decreases with the distance from the inlet, due to coalescence during flow development, (iii) the wave velocity increases with gas superficial velocity and marginally increases with liquid superficial velocity and (iv) the wave amplitude decreases with gas superficial velocity and increases with liquid superficial velocity. Similar observations were presented by Han et al. (2006) and Wang et al. (2019), using

parallel wire probes in adiabatic air-water flows. Besides that, Han and coworkers highlighted that due to the high velocity of the waves, they can transport up to 80% of the total liquid mass flux. Lee et al. (2017) and Su et al. (2019) used conductance sensors in flows with varying temperature and under diabatic conditions, respectively. While Lee and coworkers only performed a feasibility test of a RI sensor designed for conditions under variable temperatures in falling films, Su and coworkers used a sensor based on triangular-shaped electrodes and related the liquid film waviness with the heated surface temperature oscillations in a 10x10mm^2 duct: regions with thick films presented higher surface temperature and lower HTCs than regions with thin films. In microchannels, D'Aleo et al. (2013) and Huang et al. (2017) investigated adiabatic air-water slug flows using conductance sensors. Unfortunately, neither annular flows nor heating conditions were studied by either group of researchers. Table 1 presents a summary of the flush-mounted sensors used in the studies cited above.

Similar to conductance sensors, the majority of studies in which δ was measured using optical techniques was performed under adiabatic conditions in conventional-sized channels (Alekseenko et al. (2015), Charogiannis et al. (2015), Vasques et al. (2018), Charogiannis et al. (2019) and Moreira et al. (2020)). Contrary to the observations of previous researchers, Moreira et al. (2020) found for their experimental conditions that the disturbance wave velocity did not increase with either vapor or liquid velocity, in fact, they observed a slight decrease for high vapor velocities. It was argued that the range of δ observed in their experiments was thinner than most previous studies and that the film flow would switch from being driven by the waves to behave as a wall-bounded single-phase flow. In microchannels, Han and Shikazono (2009, 2010) evaluated δ for air-water adiabatic slug flows using LFDM (Laser Focus Displacement Meter), a technique that evaluates the thickness based on the reflection at the gas-liquid interface. The authors provided relations to predict δ at the bubble nose that depended on the capillary number, ($Ca=\mu U/\sigma$), defined based on the bubble velocity. Han et al. (2012) performed measurements of δ under heating conditions for both pure ethanol and pure water. Although annular flows were observed in their study, the focus was on the effect of the heat flux on the film that formed between the gas bubbles and the channel wall during slug flows. Later, Han et al. (2015) measured δ in adiabatic air-water annular flows, proposing a correlation to predict the average δ based solely on their own data. They did not evaluate the waves frequency and velocity due to limitations of their experimental apparatus. Similarly to Han and Shikazono (2009), Patel et al. (2017) and Bartkus and Kuznetsov (2019) related δ, measured with fluorescence-based techniques for air-water slug flows in microchannels, with the capillary number.

Although δ has been evaluated for microchannels, most studies focused on adiabatic slug flows and mean film thicknesses, not evaluating wave frequency, velocity and amplitude. The correlations for δ developed by Han and Shikazono (2009, 2010) were used by Magnini and Thome (2017) in their updated 3-zone model for diabatic slug flows in microchannels. The 3-zone model divides the slug flow into the periodic passage of a liquid slug followed by a bubble, with a dry zone at the tail of the bubble occurring or not depending on the heating conditions. In the bubble zone, the HTC is calculated by thermal conduction through the liquid film ($h=k/\delta$). Magnini and Thome validated the model with CFD simulations and experimental data. The CFD comparison showed that the model captured the periodic behavior of the slug flow effectively and the experimental data comparison showed that the tendency of the mean HTC predicted by the model was in accordance with the experiments. However, the 3-zone model is not applicable to annular flows. Rather, the model developed by Cioncolini and Thome (2016) is for annular flows. Although the model provides good predictions for macrochannels, deviations are observed between predicted values and experimental data for microchannels, especially for intermediate to high vapor qualities in non-circular channels, conditions where dryout is likely to occur.

In this context, the present paper concerns a theoretical analysis of conductance sensors designed for the evaluation of δ in microchannels under heating conditions. The objective is to use this sensor to characterize the liquid film in terms of mean thickness, waves frequency, amplitude, and velocity during annular flows of water in a square channel of 1x1mm^2 under heating conditions near to wall dryout. According to the literature review presented in this paper, experimental data on wave structure for annular flows in microchannels are not available. Since the sensor geometry dictates its range of measurements, firstly, methodologies from the literature are employed to evaluate the mean δ for various mass velocities and a broad range of vapor quality. Then, numerical simulations of different sensor geometries are presented, pointing out the aspects that must be dealt with when diabatic conditions are investigated.

Table 1 - Summary of recent works that used conductance sensors mounted flush to the wall

	Author	Sensor size	Smallest measurement	Heating
Macro	Damsohn and Prasser (2009)	3.12 x 3.12 mm^2	~25 μm	No
	Zhao et al. (2013)	Ø 13.4 mm	~100 μm	No
	Tiwari et al. (2014)	2 x 2 mm^2	~100 μm	No
	Lee et al. (2017)	Ø 4.5 mm	Not reported	No. But temperature was varied
	Su et al. (2019)	2.5 x 5 mm^2	~150 μm	Yes
Micro	D'Aleo et al. (2013)	495 x 230 μm^2	<5 μm	No
	Huang et al. (2017)	Ø 310 μm	<5 μm	No

2. FILM THICKNESS PREDICTIONS

To guide the design of the sensor, firstly δ was estimated based on the following approaches: (i) estimation of the fraction of liquid flowing as film; (ii) adopting a turbulence model for the film as proposed by Cioncolini et al. (2015), and; (iii) based on a prediction method for the liquid film thickness in microchannels under adiabatic conditions. The literature review revealed that the majority of studies concerning the experimental evaluation of δ under microscale conditions focused on adiabatic slug flows rather than diabatic annular flows, thus the above approaches have not been validated against experimental data under these conditions. The implemented approaches are detailed in the following sections.

2.1 Liquid Phase Fraction within the Film

In this approach, the void (ε) and entrainment (e) fractions of the flow were estimated according to the methods of Kanizawa and Ribatski (2016) and Cioncolini and Thome (2012), respectively. Assuming homogeneous flow along the vapor core, the hold-up of liquid droplets (γ) in the vapor core is related to ε, e and the vapor quality (x). Then, δ is calculated assuming that the film is uniform along the perimeter of the duct.

2.2 Liquid Film Turbulence Model

Based on pressure drop and mean film thicknesses evaluated experimentally and an indirect assessment of turbulence in the liquid film, Cioncolini et al. (2015) proposed transition boundaries to determine laminar, buffer and turbulent layers in the liquid film flow, according to the film flow Reynolds number (Re_{lf}). The transition boundaries were determined as follows. The laminar-buffer layer transition was determined from Ashwood et al. (2015) liquid film velocity profiles and assuming that the film flow was analogous to single-phase boundary layer flows. When the dimensionless velocity was equal to the dimensionless distance from the wall ($V^+=y^+$), the region was laminar. The buffer-turbulent layer transition was determined based on the ratio (R) between laminar film flow rate, calculated by solving the momentum equation for the film, and the experimental film flow rate. When *R* was larger than one, the region was turbulent. The mean δ is then related to (Re_{lf}).

2.3 Film Thickness Prediction Method

The method developed by Han et al. (2015) was chosen, because it was developed based on liquid film thicknesses measured in rectangular microchannel during annular flows. The measurement technique was the LFDM which, according to the authors, allows for uncertainties lower than 0.01μm. Their prediction method was developed based on a separate flow model, considering a force balance on the film and the vapor core and assuming a flat vapor-liquid interface.

The three approaches require iterative solutions, which were carried out in MatLab 2015a. Figure 1 shows liquid film thickness predictions for flow of water at 100°C for mass velocities of 100, 300 and 500 kg/m^{2}s. According to this figure, the methodologies/approaches (i) and (iii) provide almost similar results independently of the flow conditions, while methodology (ii) provides results that become close to the predictions given by the other approaches as the mass velocity and vapor quality increase. The boxes inside each figure show close looks of the regions of the plots where dryout inception is likely to occur, according to the method of Kim and Mudawar (2013b), corresponding to film thicknesses lower than 10μm. It must be pointed out that: (i) the predictions based on the above mentioned approaches present errors which ultimately lead to uncertainties on the liquid film thickness estimations, and; (ii) the methodologies provide mean values, neglecting the non-uniformity of the film thickness along the channel perimeter and the waviness of the film which amplitude may be assumed of the same order of its mean thickness.

For a given combination of mass velocity, vapor quality, duct geometry and fluid properties, the variables that determine the film thickness in methodology (i) are e and ε and in methodology (ii), e and τ_w. In this sense, the film thickness uncertainties were determined by propagating the uncertainties in the estimation of these variables. It was assumed that the uncertainty of each variable was equal to the mean relative errors of the original methods employed for their predictions, as reported by the respective authors, viz. 1.8% for void fraction (Kanizawa and Ribatski (2016)), 6.8% for entrainment fraction (Cioncolini and Thome (2012)) and 17.2% for wall shear stress (Kim and Mudawar (2013a)). The mean relative errors were calculated based on the experimental database used to develop each correlation. For methodology (iii) the uncertainty was not estimated, because Han and coworkers did not report the mean error of their method compared to their experimental results. The uncertainties estimations are shown in Fig. 2.

From this analysis, it was found that the uncertainty obtained through methodology (i) is mainly due to the void fraction. Although the uncertainty on the estimation of the void fraction is low, it produces large uncertainties on the liquid film thickness: the uncertainty is 4.5μm for the vapor qualities and mass velocities shown in Fig. 2. To reduce the uncertainty below 1μm, the void fraction uncertainty would have to be reduced to 0.4%. Regarding methodology (ii), the parameter that dominated the uncertainty propagation was the shear stress. As the mass velocity was increased, the entrainment fraction increased, and then both parameters provided comparable effects on the overall uncertainty. If the

method used for calculating the shear stress had an error of 10%, the uncertainty in the thickness estimation would be kept below 10%.

If the upper bound limit of the film thickness is chosen as the maximum of the predictions considering the uncertainty propagation, a maximum thickness of 16μm is expected. Based on this analyses and considering the amplitude of the interfacial waves, it can be concluded that is necessary to develop a sensor capable of evaluating thicknesses ranging from 0 to 32μm in order to measure thin films close to the dryout condition.

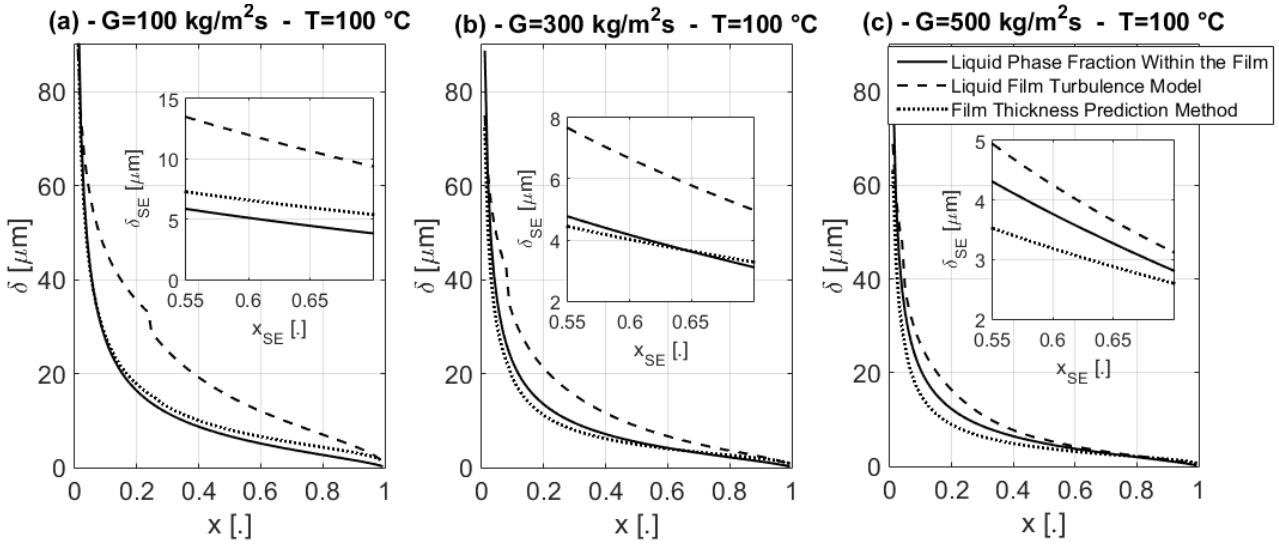

Figure 1. Film thickness behavior predicted according to the methodologies (i) - Liquid Phase Fraction within the Film, (ii) - Liquid Film Turbulence Model and (iii) - Film Thickness Prediction Method, for: (a) G=100kg/m²s, (b) G=300kg/m²s and (c) G=500kg/m²s.

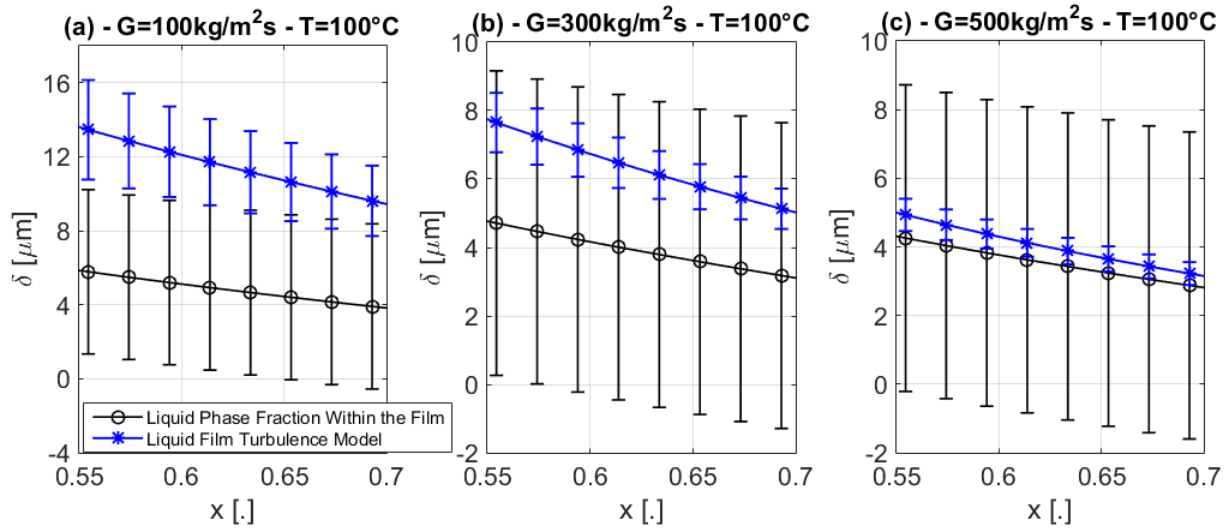

Figure 2. Uncertainty of the film thickness estimated according to methods (i) – Liquid phase fraction within the film, and (ii) – Liquid film turbulence model, for: (a) G=100kg/m²s, (b) G=300kg/m²s and (c) G=500kg/m²s.

3. SENSOR SIMULATIONS

Numerical simulations were performed through ANSYS Electronics 2019 to investigate the influence of the geometry on the electrical behavior of the sensor (δ vs electric signal curve). The simulation domain was a water plate whose thickness was varied (in the Z direction), with the sensors modelled as 2D elements at its bottom face (XY plane). With exception of the area occupied by the electrodes, where the excitations were imposed, every face of the water element was electrically insulated. The thickness of the sensors was not considered in any simulation presented in this work, because they did not affect the electric signal appreciably and increased the computational time. Figures 3a and 3b display the geometries of the flush-mounted conductance sensors proposed by Huang et al. (2017) and Damsohn and Prasser (2009), named Ring-Island (RI) and Island-Island (II), respectively, along with the simulated results considering geometries with and without guard electrodes. This figure displays the curves of δ vs electrical current for an excitation

of 4V DC and assuming the water electrical conductivity as 200µS/cm. A comparison of the results in Fig. 3a and 3b reveals the following: (i) RI produces a higher intensity signal; (ii) RI is more sensitive for very thin films (for δ<5µm the curve of RI is steeper than for II); (iii) RI saturates for lower film thicknesses, and (iv) the effect of the addition of ground electrodes is more intense in II sensors, with the electrical signal corresponding to less than of the half the signal without guard electrodes. Therefore, based on this analysis and on the estimated results for the film thickness, it is possible to conclude that the RI geometry is more appropriate for the evaluation of the film thickness in microchannels under conditions close to the dryout, due to the higher sensitivity and signal-to-noise ratio for thin films. Even though the guard electrodes do not show an appreciable influence for thin films, they must be used to reduce crosstalk between adjacent sensing elements. The inputs of the simulations are presented in Table 2 and the details of the geometries of each sensor are given in the figures.

The convergence history of the simulation of the sensor depicted in Fig. 3a, blue solid line, is presented in Fig. 4, for δ=5µm. Similar results were obtained for all conditions simulated. The default adaptive mesh scheme from Ansys Electronics was used for meshing, it performs the error analysis in the simulated domain and refines the mesh in areas where the error of the solution is larger. In Fig. 4, the solution needed 25 passes, with 35% increase in the number of elements between passes, to converge the solution within the tolerance of 10^{-3}. This led to over 350000 discrete elements. After each pass, the software calculates an energy value based on the error of the solution and compares it with the energy calculated based on the sources (excitations). The actual procedure implemented for this is an internal tool of the software. The change in the total energy after each pass is also calculated and is reported as the Delta Energy (%). When both Delta Energy and Energy Error are below the tolerance, the solution has converged.

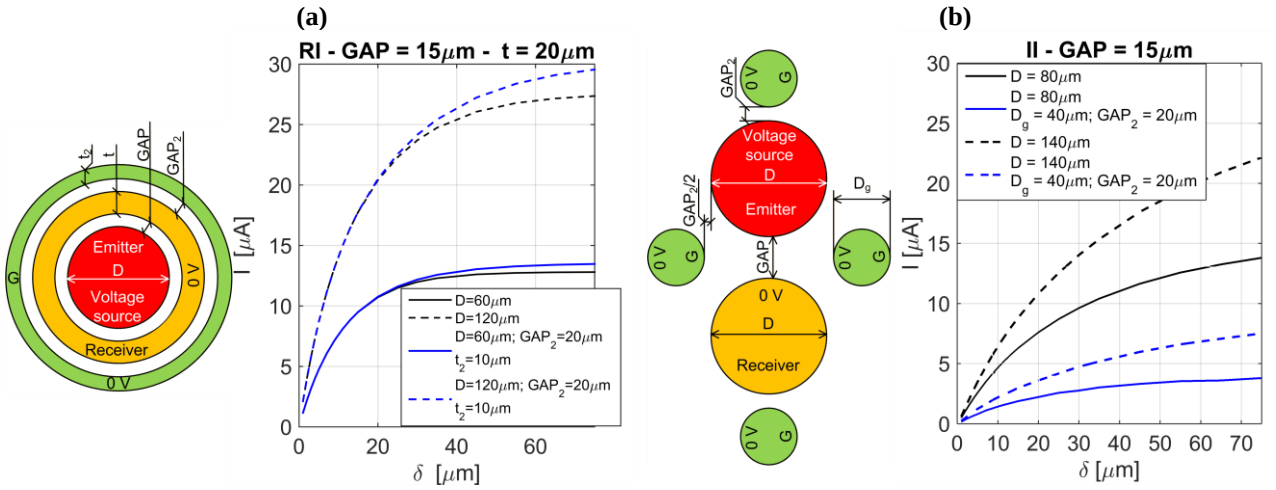

Figure 3. Starting geometries for numerical simulations and simulated results. (a) Ring-island (RI); (b) Island-island (II). Black lines are for sensors without guard electrodes and blue lines are for sensors with guard electrodes.

Table 2 - Simulations inputs

Geometry	Film Electrical Conductivity	Tolerance	Boundary Conditions	
Described in Figures	200µs/cm	10^{-3}	Emitter	4V
			Receivers	0V
			Guard	0V
			Other Surfaces	Insulated

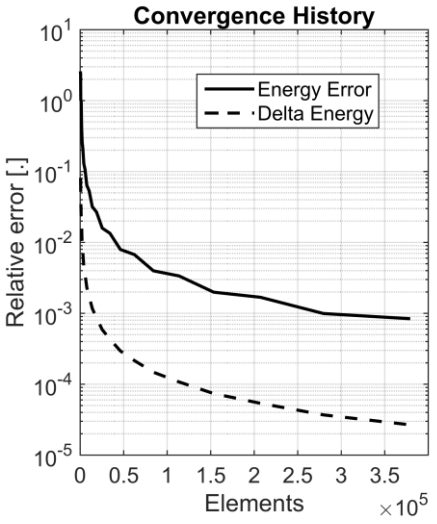

Figure 4. Convergence history of the solution for one case

3.1 Sensor Calibration

When measuring liquid film thickness care should be exercised on the calibration of the sensor. Usually, this involves a procedure of deriving experimentally a relationship for the film thickness (which value is known) vs electric signal curve. In sensors based on the liquid film conductance, based on the fact that the liquid conducts electricity and the vapor does not, the calibration is done by placing a non-conductive plate parallel to the sensor at a known distance, forming a dummy channel. The height of the dummy channel emulates the film thickness, as shown in Fig. 5. The calibration curve is obtained filling the channel with water, varying its height, and relating it with the electrical signal on each sensing element. Damsohn and Prasser (2009), D'Aleo et al. (2013), Lee et al. (2017) and Su et al. (2019) used a calibration device similar to the one shown in Fig. 5a, where the height of the dummy channel is varied manually or using a step motor and measured by a micrometer screw. Huang et al. (2017) used a different approach, shown in Fig. 5b, where the dummy channel was formed by joining the sensor with U-shaped components, forming dummy channels with different heights. During the calibration process, the liquid electrical conductivity is monitored.

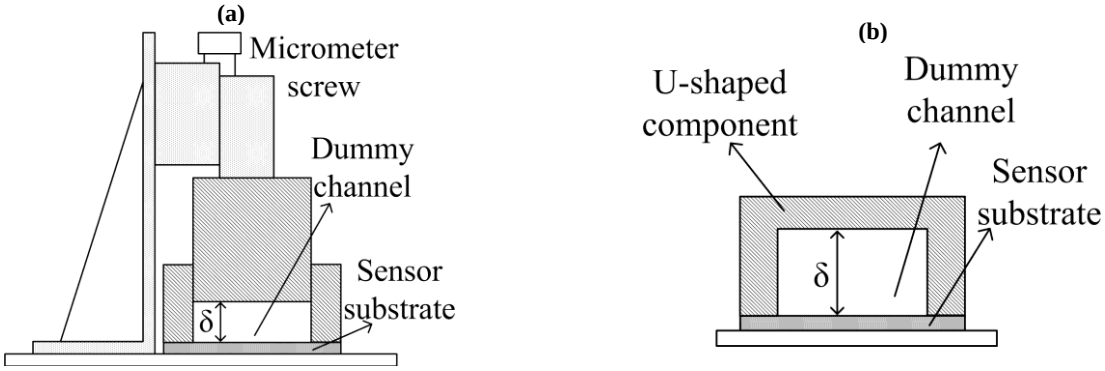

Figure 5. Calibration devices for liquid film thickness sensors. (a) With micrometer screw to vary channel height. (b) With U-shaped component to vary channel height

3.2 Analysis of the Effect of the water electrical conductivity on the sensor signal

The accurate evaluation of the electrical conductivity of the water is necessary to relate the sensor signal to δ during experiments. The sensor signal varies linearly with the liquid electrical conductivity because only conduction effects are measured. In air-water adiabatic experiments, the electrical conductivity is monitored at the inlet of the test section by an electrical conductivity meter and the temperature of the liquid is evaluated at the inlet and outlet of the test section. Usually, the temperature variations are negligible, and no evaporation occurs during the tests, so the electrical conductivity is assumed constant along the test section. To interpret the data, the ratio between the conductivity during experiments and during calibration is used to correct the electrical signal to be input in the calibration curve and converted to film thicknesses. However, under diabatic conditions, this solution cannot be employed because both evaporation and temperature variations along the flow path affect water electrical properties. For instance, in flow boiling of water in a $1x1mm^2$ square duct where dryout incipience is observed at the outlet of the duct, the temperature difference between inlet and outlet can be as high as 40°C in a 150mm length, due to the high pressure drop evaluated according to the method of Kim and Mudawar (2013a). This precludes the use of a single conductivity measurement at the inlet of the test section. Coney (1973), in his theoretical analysis of conductivity sensors for liquid film thickness evaluation, proposed two solutions to overcome this problem: (i) measuring the *in-situ* conductivity by diverting part of the liquid film to a region where its conductivity can be evaluated, or; (ii) using a sensor with more than one receiver per emitter and evaluate the ratio between currents in each receiver (I_o/I_i – *i* refers to inner and *o* to outer). Option (ii) seems to be more suitable for microchannels since the liquid film is not perturbed.

Lee et al. (2017) developed a sensor for conventional-sized channels following the option (ii) with two rings for one island, as shown in Fig. 6a. The sensors were fabricated in a flexible printed-circuit board with 30μm thick copper electrodes covered with a thin gold layer to protect them from oxidation. These authors observed that: (i) for a film thickness of 3mm (close to the sensor saturation), the uncertainty in the measurement of the current ratio produced an uncertainty of 5.7% in the determination of the film thickness, with this value decreasing below 1.6% for thicknesses below 1.5mm, and; (ii) several calibrations performed in the temperature range of 20 to 40°C presented average deviations of 3.9% in the current ratio, even though the current to each receiver varied more than 40%, proving that the current ratio can minimize the effects of the electrical conductivity variations. Some differences between simulated and experimental results were observed: the current ratio measured experimentally was higher than the simulated value and the curve did not vanish as the film thickness tended to zero. They credited those deviations to the circuitry impedance, fabrication imperfections or a thin liquid layer that remained above the sensor when the calibration device contacted the electrodes during the calibration procedure shown in Fig. 5a. Based on the results of Lee et al. (2017) and the analysis from Coney

(1973), the designs shown in Fig. 6b and 6c are proposed in the present study for microchannels and their performance evaluated through numerical simulations. These designs consider guard electrodes outside the outer ring to reduce crosstalk and interferences from neighboring electrodes. Sensors like the ones shown in Fig. 6 may be fabricated in gold by microfabrication processes, whose main processes are: deposition of the photoresist on a silicon wafer; patterning of the electrodes shapes on the substrate with photolithography; deposition and lift-off of the gold; deposition of an insulation layer to keep only the electrodes exposed. With these processes, the thickness of the electrodes is kept between 150 and 200nm.

The placement of the electrodes changes the behavior of the sensors as well as the magnitude of the currents that flow to each receiver. The value of I_o/I_i or V_r will increase or decrease with the thickening of the liquid film depending on which electrodes are chosen as receivers and emitter and to the electrodes sizes and spacings. To evaluate the trend and the influence of each dimension on the current ratio curve, simulations were performed with only one dimension varied at a time, keeping the others fixed. The fixed values were D=100µm, $GAP_1=t_1=GAP_2=t_2=20$µm and the variations were 50µm <D<150µm and 10µm<GAP_1, t_1, GAP_2, t_2<50µm. Figure 7 shows simulated results for the sensors depicted in Figs. 6a and 6b for various diameters of the island. In the case of the sensor displayed in Fig. 6a, the outer ring current is rather small compared to the inner ring current, close to 10^{-9}A for thin films, and the signal-to-noise ratio is too low, increasing the uncertainty of its measurements. Also, due to the low values of I_o, the current ratio is close to zero for thin films, as shown in Fig. 7c. In these conditions the errors could become unbearable. In the case of the sensor from Fig. 6b, the currents flowing to both receivers are of the order of 10^{-6}A, increasing the signal-to-noise ratio of both measurements, especially for the outer current in the thin film region.

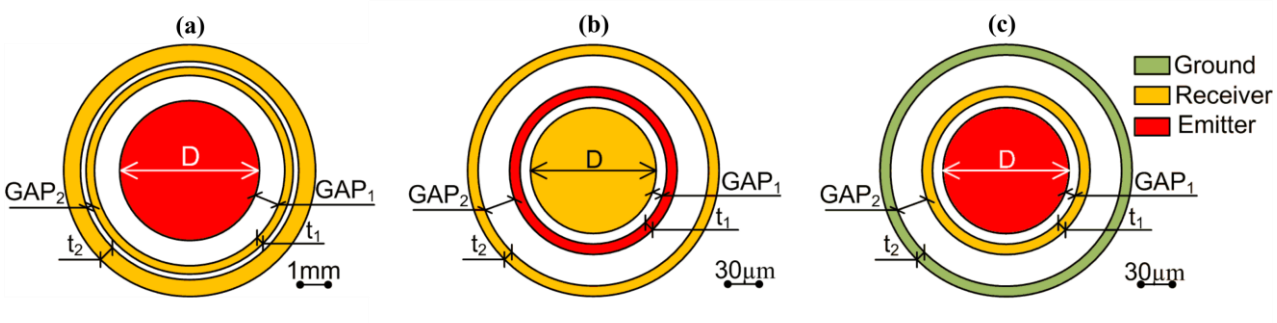

Figure 6. Sensors for conditions where electrical conductivity of the liquid varies along the flow path. (a) Lee et al. (2017) for macrochannels; (b) and (c) proposed geometries for microchannel. The scale of each geometry is shown at the inferior right side of the figure

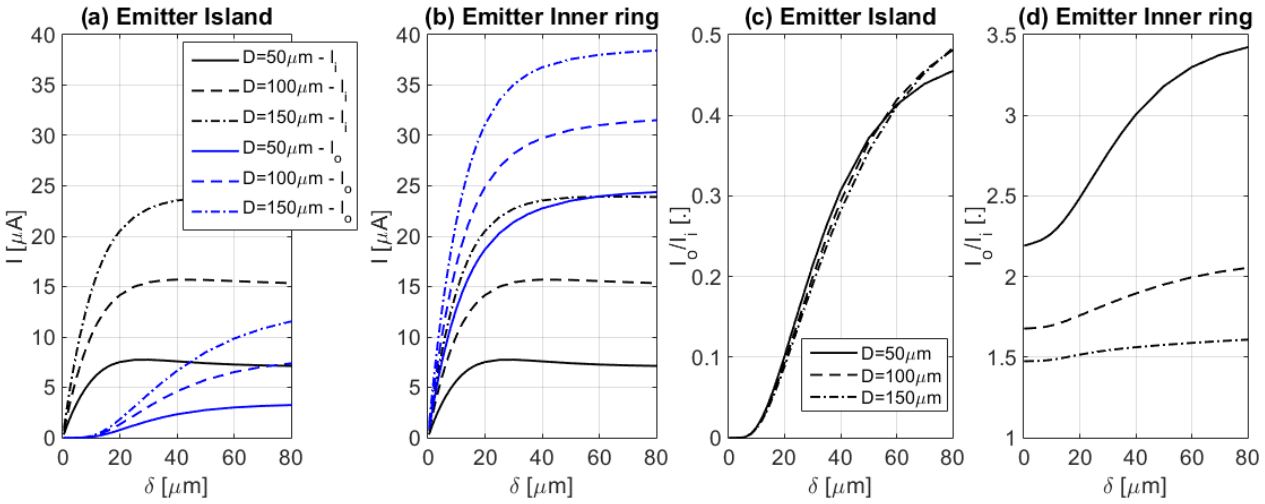

Figure 7. Electrical currents to each receiver (a-b) and current ratio (c-d) for varying island diameters when $GAP_1=t_1=GAP_2=t_2=20$µm: (a) and (c) the island is the emitter and the rings are the receivers, and; (b) and (d) the inner ring is the emitter and the island and the outer ring are the receivers

Further numerical simulations showed that when the island is the emitter the dimensions t_1 and GAP_2 influenced the most the sensor response, as shown in Fig. 8a, 8b, 8d and 8e. Varying their values influenced the whole range of measurements of the sensor: increasing t_1 enlarges the inner ring and moves the outer ring further away from the island while increasing GAP_2 moves the outer ring further apart, thus I_i increases and I_o decreases. The other variables had noticeable impacts only for thick films (~30µm). Neither variable affected considerably the response for films below

10µm, the outer current remained below 1µA and the current ratio below 0.1. When the inner ring is the emitter, all the dimensions have a considerable impact on the current ratio, but GAP_1 and GAP_2 define the shape of the curve: when $GAP_1/GAP_2>>1$, I_o/I_i decreases rapidly for thin films, reaches a minimum and then increases smoothly till saturation or remains constant depending on the other dimensions of the sensor; when $GAP_1/GAP_2<<1$, I_o/I_i increases for thin films till it asymptotically reaches the saturation value for thick films. It is important to highlight that the measurements performed by the design shown in Fig. 6c is based on a single voltage signal, V_r. Voltage is applied to the island, while the outer ring is grounded. The inner ring is connected to a high impedance channel, so the electric field established between the island and the outer ring is not disturbed while V_r is measured. Placing the inner ring closer to the island provides a voltage that decreases as the film gets thicker, while placing the inner ring closer to the outer ring provides a voltage that increases as the film gets thicker. The behavior of the sensor is similar to the behavior of the sensor in Fig. 6b, since they act as electric current and voltage dividers, respectively, and the electric resistance is the film, which is the same for both cases.

According to the results illustrated in Figs. 7 and 8, for thin film measurements the best choices are the inner ring as the emitter and the solution based on a single voltage measurement, depicted in Figs. 6b and 6c. These solutions, in comparison with the geometry of Fig. 6a, provide signals that do not vanish as the thickness tends to zero, higher intensity signals and higher sensitivity for thin films. Simulating various combinations of parameters, the selected geometry was chosen with the following dimensions: D=120µm, GAP_1=10µm, t_1=10µm, GAP_2=30µm and t_2=10µm. This geometry was selected not only because of its current ratio curve, but also because the magnitude of the current to each receiver seems reasonable not be dominated by electrical noise at the thin film region. It should be expected that additional improvements in the design are probable after the fabrication and test of prototypes. Figs. 9a and 9b show the simulated results for the selected geometry for a sensor based on current ratio measurement and Fig. 9c shows the results for a sensor based on voltage measurement in the inner ring, Fig. 9c.

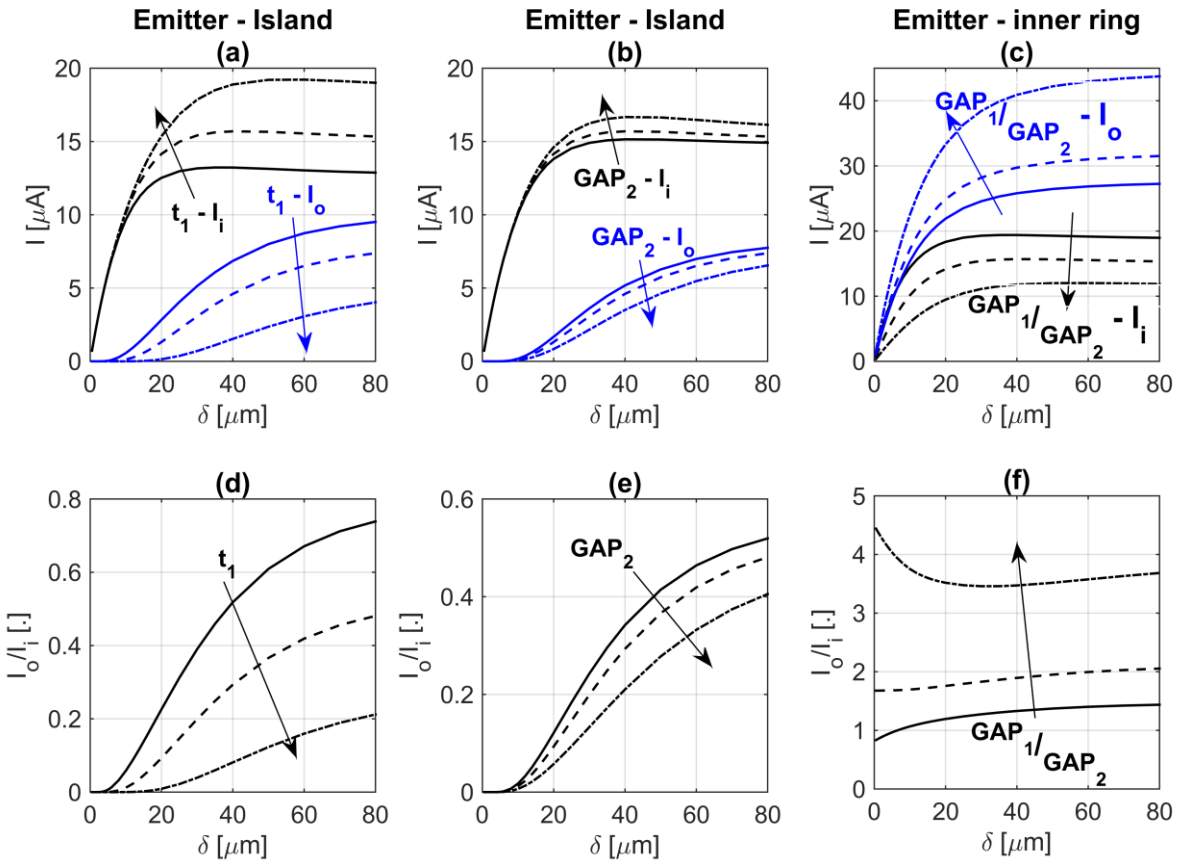

Figure 8. General trends observed for the current ratio and influences of the most important parameters in each design: (a-c) inner and outer currents and (d-f) current ratio. The arrows indicate that the variable value is increasing.

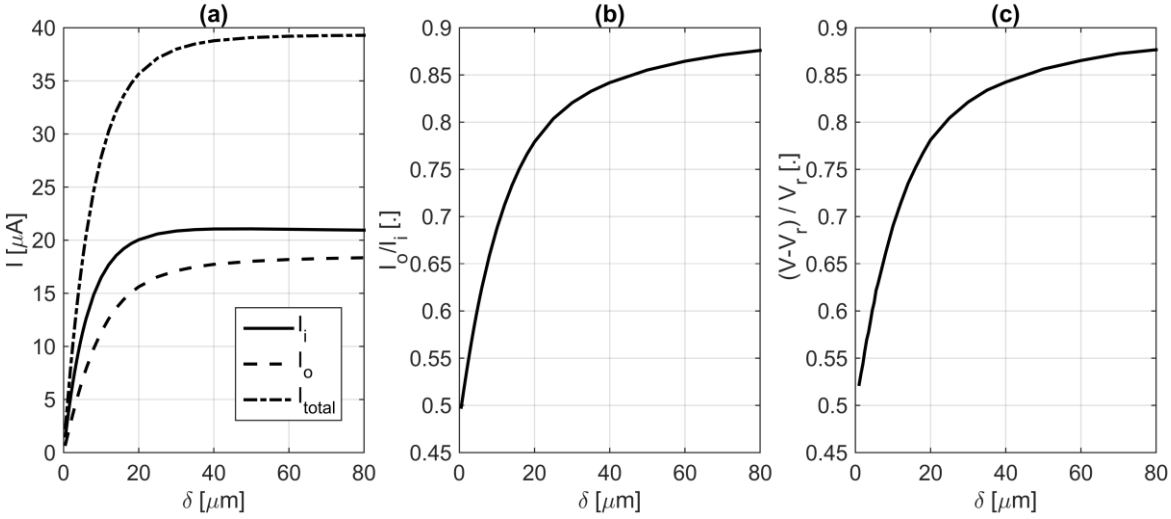

Figure 9. Simulated results for the sensor depicted in Fig. 6b and 6c. (a) current to each electrode for sensor in Fig. 6b; (b) current ratio for sensor in Fig. 6b; (c) non-dimensional voltage V_r for sensor in Fig. 6c.

4. CONCLUSIONS

A theoretical analysis of conductance sensors for measuring liquid film thickness in microscale annular flows was presented. Focusing on sensitivity and signal intensity, the analysis showed that interdigitated sensors are more adequate to evaluate thin films due to higher dI/dδ and higher currents for a given voltage and electrical conductivity of the liquid, but they saturate for thinner films and occupy larger areas of the substrate, reducing the spatial resolution of the measurement. The dependence of the electrical current on the electrical conductivity of the liquid was considered and three different designs of liquid film thickness sensors were illustrated, each one with its measurement independent of conductivity changes. Only Lee et al. (2017) used such sensors, but in macroscale applications. Since this concept of conductance sensors have not yet been used in microscale applications and the electrical noise is difficult to quantify theoretically, the geometry selected still needs testing and additional improvement if necessary. Regarding the values of the excitation and electrical conductivity of the water in the numerical simulations, the data of D'Aleo et al. (2013) were considered, which can be optimized after testing the prototypes.

5. ACKNOWLEDGEMENTS

The authors gratefully acknowledge the financial support from FAPESP (São Paulo Research Foundation) through a Thematic and a Scholarship grants under contract numbers 2016/09509-1 and 2019/01755-1, respectively. The second author also acknowledge the support of CNPq (National Counsel of Technological and Scientific Development of Brazil) under Contract Numbers 305673/2017-3. This study was financed in part by the Coordenação de Aperfeiçoamento de Pessoal de Nível Superior - Brasil (CAPES) - Finance Code 001.

6. REFERENCES

Alekseenko, S. V., Cherdantsev, A. V., Cherdantsev, M. V., Isaenkov, S. V., Markovich, D.M., 2015. Study of formation and development of disturbance waves in annular gas-liquid flow. Int. J. Multiph. Flow 77, 65–75.

Ashwood, A.C., Hogen, S.J. Vanden, Rodarte, M.A., Kopplin, C.R., Rodríguez, D.J., Hurlburt, E.T., Shedd, T.A., 2015. A multiphase , micro-scale PIV measurement technique for liquid film velocity measurements in annular two-phase flow. Int. J. Multiph. Flow

Bartkus, G. V., Kuznetsov, V. V., 2019. Experimental investigation of gas-liquid flow characteristics in slit rectangular and circular channels. J. Phys. Conf. Ser. 1382, 0–6

Charogiannis, A., An, J.S., Markides, C.N., 2015. A simultaneous planar laser-induced fluorescence , particle image velocimetry and particle tracking velocimetry technique for the investigation of thin liquid-film flows. Exp. Therm. Fluid Sci. 68, 516–536.

Charogiannis, A., Sik An, J., Voulgaropoulos, V., Markides, C.N., 2019. Structured planar laser-induced fluorescence (S-PLIF) for the accurate identification of interfaces in multiphase flows. Int. J. Multiph. Flow 118, 193–204.

Cioncolini, A., Del, D., Thome, J.R., 2015. An indirect criterion for the laminar to turbulent flow transition in shear-driven annular liquid films. Int. J. Multiph. Flow 75, 26–38.

Cioncolini, A., Thome, J.R., 2012. Entrained liquid fraction prediction in adiabatic and evaporating annular two-phase flow. Nucl. Eng. Des. 243, 200–213.

Coney, M.W.E., 1973. The theory and application of conductance probes for the measurement of liquid film thickness in two-phase flow. J. Phys. E. 6, 903–910.
D'Aleo, F.P., Papadopoulos, P., Prasser, H.M., 2013. Miniaturized liquid film sensor (MLFS) for two phase flow measurements in square microchannels with high spatial resolution. Flow Meas. Instrum. 30, 10–17.
Damsohn, M., Prasser, H.-M., 2009. High-speed liquid film sensor for two-phase flows with high spatial resolution based on electrical conductance. Flow Meas. Instrum. 20, 1–14.
Han, H., Zhu, Z., Gabriel, K., 2006. A study on the effect of gas flow rate on the wave characteristics in two-phase gas-liquid annular flow. Nucl. Eng. Des. 236, 2580–2588.
Han, Y., Kanno, H., Ahn, Y.J., Shikazono, N., 2015. Measurement of liquid film thickness in micro tube annular flow. Int. J. Multiph. Flow 73, 264–274.
Han, Y., Shikazono, N., 2010. The effect of bubble acceleration on the liquid film thickness in micro tubes. Int. J. Heat Fluid Flow 31, 630–639.
Han, Y., Shikazono, N., 2009. Measurement of liquid film thickness in micro square channel. Int. J. Multiph. Flow 35, 896–903.
Han, Y., Shikazono, N., Kasagi, N., 2012. The effect of liquid film evaporation on flow boiling heat transfer in a micro tube. Int. J. Heat Mass Transf. 55, 547–555.
Huang, H., Dhir, V.K., Pan, L. ming, 2017. Liquid film thickness measurement underneath a gas slug with miniaturized sensor matrix in a microchannel. Microfluid. Nanofluidics 21, 1–13.
Kang, H.C., Kim, M.H., 1992. The development of a flush-wire probe and calibration method for measuring liquid film thickness. Int. J. Multiph. Flow 18, 423–437.
Kanizawa, F.T., Ribatski, G., 2016. Void fraction predictive method based on the minimum kinetic energy. J. Brazilian Soc. Mech. Sci. Eng. 38, 209–225.
Kim, S.M., Mudawar, I., 2013a. Universal approach to predicting two-phase frictional pressure drop for mini/micro-channel saturated flow boiling. Int. J. Heat Mass Transf. 58, 718–734.
Kim, S.M., Mudawar, I., 2013b. Universal approach to predicting saturated flow boiling heat transfer in mini/micro-channels – Part I. Dryout incipience quality. Int. J. Heat Mass Transf. 64, 1226–1238.
Lee, K.B., Kim, J.R., Park, G.C., Cho, H.K., 2017. Feasibility test of a liquid film thickness sensor on a flexible printed circuit board using a three-electrode conductance method. Sensors (Switzerland) 17.
Magnini, M., Thome, J.R., 2017. An updated three-zone heat transfer model for slug flow boiling in microchannels. Int. J. Multiph. Flow 91, 296–314.
Patel, R.S., Weibel, J.A., Garimella, S. V., 2017. Characterization of liquid film thickness in slug-regime microchannel flows. Int. J. Heat Mass Transf. 115, 1137–1143.
Ribatski, G., Cabezas-Gómez, L., Navarro, H.A., Saíz-Jabardo, J.M., 2007. the Advantages of Evaporation in Micro-Scale Channels To Cool Microeletronic Devices. Rev. Eng. Térmica 6, 34.
Sawant, P., Ishii, M., Hazuku, T., Takamasa, T., Mori, M., 2008. Properties of disturbance waves in vertical annular two-phase flow. Nucl. Eng. Des. 238, 3528–3541.
Su, G.Y., D'Aleo, F.P., Phillips, B., Streich, R.M., Al-Safran, E., Buongiorno, J., Prasser, H.M., 2019. On the oscillatory nature of heat transfer in steady annular flow. Int. Commun. Heat Mass Transf. 108, 104328.
Thome, J.R., Cioncolini, A., 2016. Unified Modeling Suite for Two-Phase Flow, Convective Boiling, and Condensation in Macro-and Microchannels. Heat Transf. Eng. 37, 1148–1157.
Tibiriçá, C.B., do Nascimento, F.J., Ribatski, G., 2010. Film thickness measurement techniques applied to micro-scale two-phase flow systems. Exp. Therm. Fluid Sci. 34, 463–473.
Tibiriçá, C.B., Ribatski, G., 2014. Flow patterns and bubble departure fundamental characteristics during flow boiling in microscale channels. Exp. Therm. Fluid Sci. 59, 152–165.
Tiwari, R., Damsohn, M., Prasser, H.M., Wymann, D., Gossweiler, C., 2014. Multi-range sensors for the measurement of liquid film thickness distributions based on electrical conductance. Flow Meas. Instrum. 40, 124–132.
Vasques, J., Cherdantsev, A., Cherdantsev, M., Isaenkov, S., Hann, D., 2018. Comparison of disturbance wave parameters with flow orientation in vertical annular gas-liquid flows in a small pipe. Exp. Therm. Fluid Sci. 97, 484–501.
Wang, G., Tang, K., Ishii, M., 2019. Film thickness and disturbance wave structure of upward annular flow. 18th Int. Top. Meet. Nucl. React. Therm. Hydraul. NURETH 2019 5193–5203.
Zhao, Y., Markides, C.N., Matar, O.K., Hewitt, G.F., 2013. International Journal of Multiphase Flow Disturbance wave development in two-phase gas – liquid upwards vertical annular flow. Int. J. Multiph. Flow 55, 111–129.

7. RESPONSIBILITY NOTICE

The authors are the only responsible for the printed material included in this paper.